Design of the Laser-Driven RF Electron Gun for the BNL Accelerator Test Facility

KIRK T. McDONALD

Abstract—The BNL electron gun will incorporate a laser-driven photocathode in the wall of a $1\frac{1}{2}$ cell RF cavity operated at a peak field of 100 MV/m. Pulses of 4.5-MeV energy, 5-ps width, and 1-nC charge will be produced with very little emittance growth due to the effects of space-charge and nonlinear RF fields. The design of the gun was aided by extensive computer simulation described here.

I. INTRODUCTION

THE Brookhaven Accelerator Test Facility (ATF), presently under construction, is a 50-MeV electron linac designed to produce electron bunches that can be synchronized with the picosecond pulse of a 100-GW CO_2 laser. This facility will be used to study the acceleration of electrons by the laser-grating technique [1] as well as by an inverse free-electron laser [2], and will also provide a picosecond source of X-rays via nonlinear Compton scattering [3]. Fig. 1 is a block diagram of the linac and laser components. Here we report on the design of the electron gun that will provide RF bunches of up to 10^{10} electrons synchronized with the laser beam.

The gun is based on the design of Fraser *et al.* [4] who incorporate a photocathode in the end wall of an RF cavity that supports a strong standing-wave field. An ultrashort laser pulse ejects a bunch of electrons into the accelerating RF field. This concept offers many advantages:

1) The electron bunch length is determined by the laser pulse width, which may be as narrow as a few picoseconds. This eliminates the need for a buncher section, and permits extremely narrow energy spreads for the accelerated beam.

2) The electron bunch is synchronized with the laser pulse to picosecond accuracy.

3) Very low emittance beams can be produced simply by decreasing the laser spot size at the photocathode.

4) The RF cavity can support acceleration gradients of order 1 MeV/cm at the cathode, minimizing the space-charge growth of the emittance when the electrons are nonrelativistic.

5) A multicavity gun can deliver a beam of several megaelectronvolts energy.

6) The gun can operate at the same RF frequency as the linac (2856 MHz for the ATF).

7) Optimum design of the RF cavity minimizes emittance growth due to nonlinear components of the transverse electric and magnetic fields.

In the design of the gun for the ATF we maximize the beam brightness by use of the highest possible accelerating field at the photocathode and the shortest laser pulse. The design parameters are summarized in Table I, and a section through the gun is shown in Fig. 2.

II. DESIGN CONSIDERATIONS

An ideal gun design would preserve the emittance of the electron bunch as it emerges from the cathode. In practice two effects blow up this initial emittance. Electromagnetic interactions among the electrons (the space-charge effect) lead to a true increase in phase-space volume, while nonlinear radial dependence of the transverse components of external electromagnetic fields lead to an apparent growth of phase volume that cannot be later corrected with linear beam optics.

The space-charge fields are only important relative to the strength of the accelerating field at the cathode. As the RF gun can have extremely large accelerating fields, only rather modest space-charge emittance growth will occur even for a relatively small bunch size. Once the electrons are relativistic, space-charge emittance growth largely ceases (as the electrons are far apart in the rest frame of the bunch). In an RF gun with a field strength of 1 MeV/cm all space-charge growth occurs within 1 cm of the cathode. The field of the image of the bunch in the cathode plane serves to compress the bunch and reduces the space-charge growth by about 30 percent in the RF gun.

Thus, the primary design feature of the gun determined by consideration of space-charge emittance growth is that the accelerating field at the cathode be large. An optimal shape for the RF cavity of the gun is suggested by the criterion that the RF fields cause minimal nonlinear distortion of the phase space of the bunch.

From a Fourier analysis of a standing-wave RF field with circular symmetry, summarized in Appendix A, we find there is an ideal form for which the transverse electric and magnetic fields have linear radial dependence. A related form for static fields [5] was the basis for the design of the Los Alamos RF gun [4]. For the RF case, it emerges
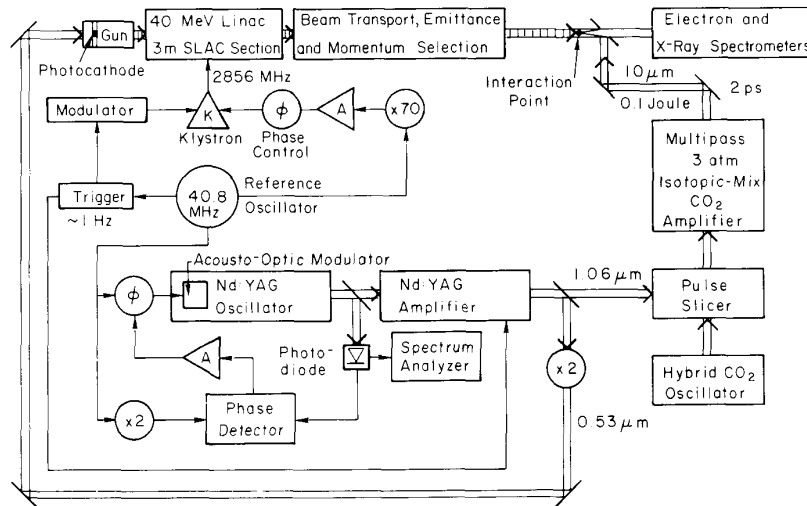
Fig. 1. Block diagram of the Brookhaven Accelerator Test Facility.

<div style="text-align:center">

TABLE I

PARAMETERS OF THE ATF GUN

</div>

RF Parameters

RF Frequency (MHz)	2856
Cathode Cell length (cm)	2.625
Second Cell length (cm)	5.23
Cell diameter (cm)	8.31
Radius of aperture (cm)	1.0
Radius of nose (cm)	1.0
Field on cathode (MV/m)	100
Peak field on wall (MV/m)	106
RF Power (MWatt)	5.9
Cavity Q	12000
RF phase for laser pulse	67°
Final beam momentum (MeV/c)	4.7

Emittance Parameters

Laser spot radius (σ in mm)	3
Laser pulse width (σ in psec)	2
Charge in bunch (nCoulomb)	1
ϵ_z[†] at cathode (mm-mrad)	3.5
$\Delta\epsilon_z$ due to self fields	6.2
$\Delta\epsilon_z$ due to rf fields	1.4
ϵ_z at exit	7.3
Beam energy spread (σ in keV)	17
Exit bunch length (σ in mm)	0.6
Exit bunch radius (σ in mm)	4.2
Exit beam angular divergence (σ in mrad)	28

[†] $\epsilon_z \equiv \dfrac{1}{mc}\sqrt{\langle x^2\rangle\langle p_z^2\rangle - \langle xp_z\rangle^2} = \sqrt{\langle x^2\rangle\langle\gamma^2\beta_z^2\rangle - \langle x\gamma\beta_z\rangle^2}.$
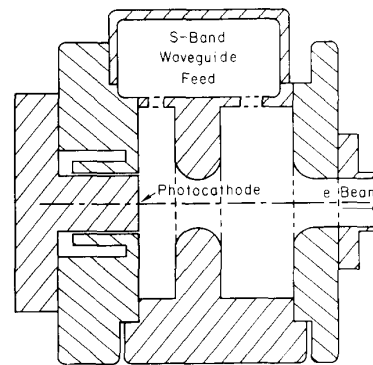

Fig. 2. Section through the RF gun. Except for the waveguide feed, the gun is axially symmetric. The $1\frac{1}{2}$-cells of the gun are 8 cm long.

that the length of a cell should be $\lambda/2$ where λ is the wavelength of the RF field, and that the fields in adjacent cells should be 180° out of phase. This is the well-known result that a "π-mode" structure causes the least distortion of the emittance of the beam.

The gun is made in a π-mode configuration by placing the cathode on a metal disk inserted at the midplane of one cell, so the first cavity is actually a half-cell, as shown in Fig. 2. The ideal geometry for the RF case permits only this location for the cathode, unlike the static case that might favor a curved cathode surface [5]. The cathode cavity is followed by as many full cells as desired, subject to power limitations. An n-cell π-mode structure supports n modes whose frequencies may be rather close unless a side-coupling scheme is used. For the ATF we will use a $1\frac{1}{2}$-cell configuration for which the mode separation is about 2 MHz out of 2856.

A π-mode configuration alone does not assure linear dependence of the transverse fields. There is an ideal shape for the cavity walls, specified in Appendix A, that

must extend to $r = \infty$. We find that a simple disk-and-washer construction provides sufficient approximation to the ideal shape so that RF-induced emittance growth will be less than that due to space charge. A more complicated construction with rounded outer walls could reduce the power consumption, but would not improve the emittance performance.

The advantage of the π-mode configuration is maximized if the electron bunch crosses a cell boundary when the electric fields vanish. Then the deflection of the beam as the bunch nears an aperture is cancelled by the opposite transverse fields encountered just beyond the entrance to the next cell. The laser pulse should strike the photocathode at an RF phase somewhat less than 90° (where 90° corresponds to maximum electric-field strength), so that the electrons leave the first cavity at a phase of 180°. The beam should already be relativistic at the exit of the cathode cavity to insure a transit time of a half-period in subsequent cells. Cell-by-cell compensation for the transverse distortions of phase space requires that each cell have the same peak field strength. The compensation is more exact the shorter the bunch.

There is no compensation for the transverse deflection at the exit of the last cell of the gun, and in practice almost all of the RF-induced emittance distortion will occur here. Edge effects at the last aperture will increase the nonlinear components of the transverse fields and slightly detune the last cell. Computer simulations of the RF gun with the program SUPERFISH [6] suggests that the edge effects are modest and the essential features of the ideal π-mode configuration can be achieved.

The transverse components of the vector potential of the RF field vanish on the cathode plane, so there is no contribution to the initial phase volume due to the electromagnetic component of the canonical momentum. In principle, if the laser field at the cathode is powerful enough it also contributes to the canonical momentum of the photoelectrons. However, this would become important only at laser intensities well above the damage threshold for the photocathode.

III. Photocathode

The photocathode should have a picosecond response time as well as good quantum efficiency, good mechanical stability, and low intrinsic emittance. In the initial operation of the ATF we will use an yttrium metal cathode to emphasize reliability; in a later phase, a Cs_3Sb cathode will be used.

The time response will be adequate if the photoelectrons can cross an optical absorption length in less than a picosecond. An electron of 1-eV energy has velocity $v/c \sim 10^{-3}$, so in 1 ps it can travel ~ 3000 Å. This is an order of magnitude greater than the absorption length of metals and of cesium-antimonide matrials (but not that of GaAs and related materials).

Tests by members of the ATF group [7] indicate that the quantum efficiency for yttrium metal illuminated by 4.65-eV light (as for a frequency-quadrupled Nd:YAG laser) is about 2×10^{-4}. The work function for yttrium is about 3.1 eV, so the photoelectrons can emerge with up to 1.5 eV. If the electrons are emitted with an isotropic angular distribution at the cathode surface this relatively high energy leads to an initial emittance of 3.5 mm · mrad, as specified in Table I. A Cs_3Sb cathode has a work function of 2.1 eV and so could be illuminated with a frequency-doubled Nd:YAG laser. As the work function of the copper walls of the RF cavity is 4.6 eV, photoemission due to scattered laser light would be less severe in this case. The quantum efficiency of Cs_3Sb can be several percent, and the initial emittance would be about a third as large as for yttrium.

The laser beam that illuminates the photocathode will derive from the Nd:YAG laser system that also provides pulses of several millijoules energy to shape the pulse of the CO_2 laser, as sketched in Fig. 1. With a quantum efficiency of 2×10^{-4}, a pulse of 25 μJ is required to eject 1 nC of charge from the cathode.

The cathode material will be deposited on a removable plug of 1-cm radius in the end face of the gun, as shown in Fig. 2. The plug will form one surface of an RF-choke joint, which avoids the need for direct electrical contact between the plug and the nearby wall of the gun. The cathode will be illuminated by a laser beam along the axis of the gun; the electron beam must be deflected away from the laser optics shortly outside the gun.

The vacuum requirements for stability of a surface over 1 day are of order 10^{-10} torr; otherwise the surface becomes coated with residual gas molecules. This is likely more critical for a cesiated cathode where a fraction of a monolayer of cesium must reside on the surface for optimal performance. Vacuum pumping will be through the RF-coupling ports, and addition ports if needed.

IV. Coupling of the RF Power

RF power at 2856 MHz will be supplied to the gun via an S-band waveguide that couples to the outer cylindrical wall of the gun, as sketched in Fig. 2. In π-mode operation the magnetic field lines circulate in opposite senses in the two cavities of the gun, and are matched to the sense of circulation in a TE_{01} mode of the waveguide. There will be essentially no coupling at all to the 0-mode of the gun.

Tests have been made with an RF model of the gun (see also Section VI) to determine the optimum configuration of the coupling holes. It appears the a $\frac{1}{2}$-in slot will allow transmission of essentially 100 percent of the waveguide power into to gun [8], when the waveguide contains a quarter-wave transformer just upstream of the gun for impedance matching. A tunable short in the waveguide just after the gun will permit balancing of the power fed to the two gun cells.

Details of the coupling are also being modelled with the 3-D code MAFIA [9].

V. SIMULATIONS OF GUN PERFORMANCE

The emittance of the gun beam has been calculated with a version of the program PARMELA,[1] modified to include ejection of low-energy electrons from a photocathode by a laser pulse.

The photoelectrons are simulated with an energy spread of a fraction of an electronvolt, and with isotropic directions. They are emitted randomly with a profile that is Gaussian in both radius and time, as for a laser pulse. The RF fields in the gun are taken from a Fourier analysis (see Appendix A) of the results of a SUPERFISH calculations. The effect of Coulomb interactions among the electrons is calculated with a point-by-point code (see Appendix B) rather than the standard code of PARMELA, as the latter seemed less suitable for very short bunches. The important effect of image charges in the cathode plane is included. PARMELA assumes cylindrical symmetry for the RF fields, but simulates a 3-D electron bunch with a small number of macroparticles (typically 400 in the present application). The simulation proceeds via a numerical integration of the equations of motion of the electron bunch, using the phase of the RF field as the time variable. We use the invariant emittance ϵ_x, defined at the bottom of Table I, to characterize the transverse phase space.

For a bunch emitted from a spot with $\sigma_r = 3$ mm with 1.5-eV initial energy, $\epsilon_x = 3.5$ mm·mrad at the cathode. This will be combined (effectively in quadrature) with emittance growth due to the RF fields near the apertures and that due to space charge.

We first explore the effect of the RF fields for a gun with peak field strength of 100 MV/m at the cathode. Fig. 3(a) shows how the emittance growth due to the RF fields alone varies with the time at which the laser pulse strikes the photocathode. The initial emittance is set to zero, and the space-charge forces are turned off. Time is measured in degrees, where $1° \sim 1$ ps at 2856 MHz, and the electric field is at a maximum at a phase of $90°$. The laser pulse length has a σ_t of 2 ps. The emittance growth is a rapid function of the initial phase and is optimized at $67°$ where the contribution to ϵ_x is only 1.4 mm·mrad. For this initial phase the bunch leaves the gun almost exactly at a phase of $360°$ as discussed above. Fig. 3(b) shows how the beam energy varies slightly with initial phase.

When the space-charge effects within the 1-nC bunch are restored they add 6.2 mm·mrad to ϵ_x, for a total of 7.3 mm·mrad at the exit of the gun. Figs. 4 and 5 show the transverse and longitudinal phase space at the exit of the gun. While the transverse phase-space area is small, it is highly elongated, with an rms angular divergence of 28 mrad and an rms radius of 4.2 mm. The large divergence requires some care in the subsequent beam transport to avoid additional emittance growth. The shape of the longitudinal phase space is perhaps not ideal; if the initial phase is increased the shape becomes more diago-
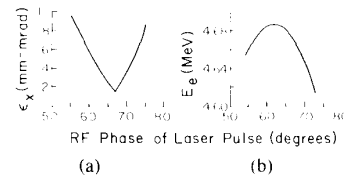
Fig. 3. (a) Emittance growth due to nonlinear transverse RF fields, and (b) final beam energy as a function of the RF phase at which the laser pulse strikes the photocathode. The laser pulse has $\sigma_r = 3$ mm and $\sigma_t = 2$ p.

nal at the expense of elongation in time, and an increase in the transverse emittance due to the RF fields.

In Fig. 6 we consider the effect of varying the laser pulse length. The bunch length at the gun exit is always proportional to the laser pulse length, and greater peak currents can be obtained with shorter pulses. However, as seen in Fig. 6(a), the beam energy spread has a minimum value of about 16 keV rms due to longitudinal space-charge blowup. Fig. 6(b) shows that there is an optimum pulse length for the transverse emittance; for very short pulses the space-charge forces become quite large, while for long pulses the RF fields cause considerable apparent emittance growth.

Fig. 7(a) shows the dependence of ϵ_x on the laser spot size. On decreasing the radius from the nominal 3 mm, the transverse emittance at first rises and then falls. In all cases the beam nearly fills the exit port of the gun, and below a spot size of 0.15 mm at the cathode there is substantial scraping of the beam. The reduction in transverse emittance for small laser spot size is obtained at the expense of longitudinal blowup of the bunch, as shown in Fig. 7(b). For very small initial spot sizes the bunch evolves into a nearly spherical shape at the exit of the gun. By moving the phase of the laser pulse slightly earlier as the initial spot size decreases, the energy spread of the beam can be kept less than 20 keV (σ).

The rms divergence of the beam on exiting the gun is shown as the dashed curve in Fig. 7(a). A minimum of about 13 mrad is achieved for an initial spot radius of 0.8 mm. If a lower beam divergence is more important than a short bunch length (i.e., high peak current), there is an option to use an initial spot size of ~ 0.5 mm. The laser intensity required would approach 100 times that for a spot size of 3 mm and might lead to surface heating of a metallic cathode, but should not be a problem for a Cs_3Sb cathode with quantum efficiency > 1 percent.

Fig. 8 considers the effect of varying the peak field strength in the RF gun. At lower fields the initial phase must be earlier for the bunch to exit at $360°$, as shown by the dashed curve. The optimal ϵ_x obtained for $\sigma_t = 2$ ps and $\sigma_r = 3$ mm is then shown by the solid curve. The individual contributions to ϵ_x from space-charge growth and nonlinear RF fields are also shown. Fields below 100 MW/m do not accelerate the bunch rapidly enough and the space-charge growth near the cathode becomes large. Above 150-MV/m field strength the nonlinear RF fields cause the dominant emittance growth.

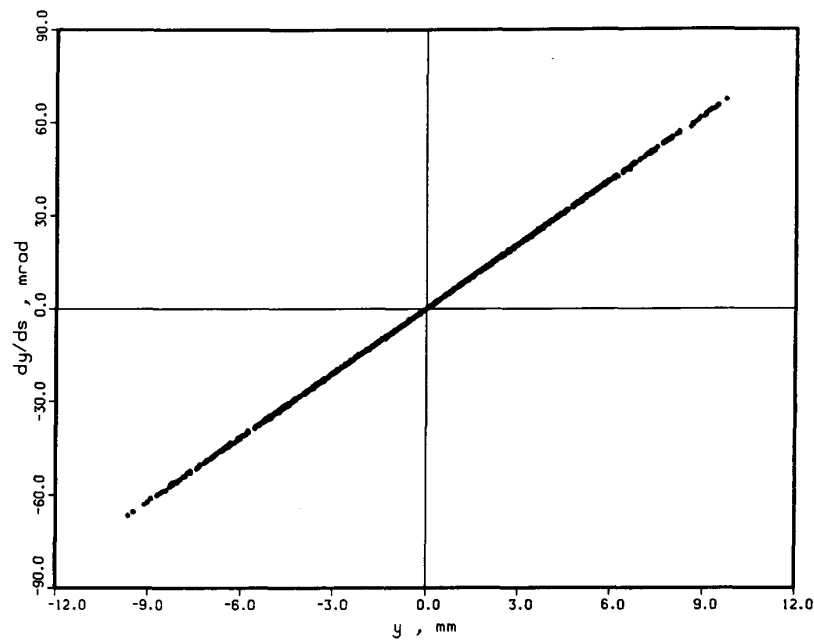Fig. 9 shows the emittance growth due to space-charge

Fig. 4. The transverse phase space at the exit of the RF gun for a bunch as given in Table I. $\sigma_x = 4.2$ mm , $\sigma_{x'} = 28$ mrad, and $\epsilon_x = 7.3$ mm $\cdot$ mrad.
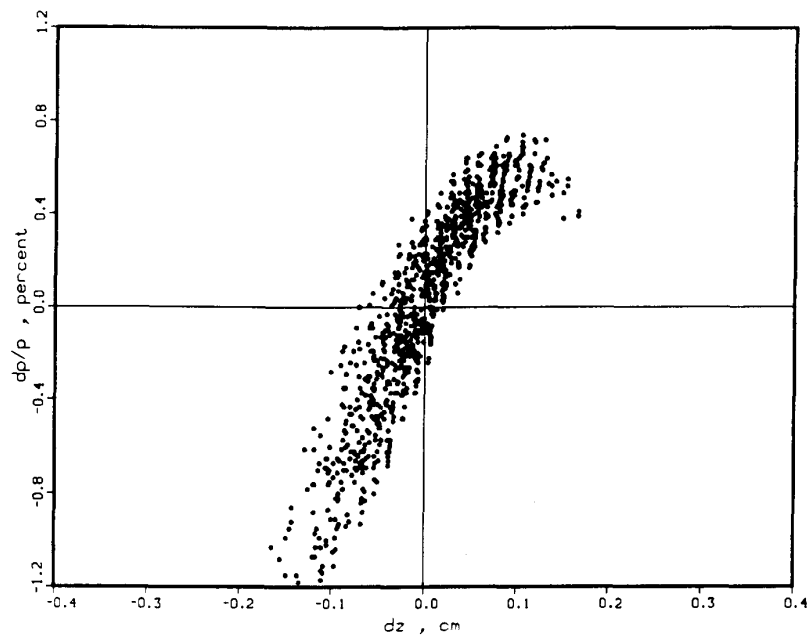

Fig. 5. The longitudinal phase space at the exit of the gun. $\sigma_z = 0.6$ mm and $\sigma_E = 17$ keV.

effects alone as a function of the total charge in the bunch. The trend is well described by $\epsilon_x \sim Q^{0.9}$. The beam brightness, which is proportional to $Q/\epsilon_x\epsilon_y$, varies with charge as $Q^{-0.8}$ in the space-charge-limited regime.

The design parameters of the RF gun seem well matched to the capabilities of this technique for producing low-emittance bunches of electrons with picosecond length. Higher fields in the gun combined with a shorter laser pulse would offer higher peak currents and greater beam energy with similar transverse emittance.

VI. TESTS WITH A FULL-SCALE RF MODEL

A model of the gun has been built in brass to study the quality and external coupling of the RF fields in the gun. The cavity Q is measured to be 5500, compared to a calculation of 12000 for actual gun which will have copper
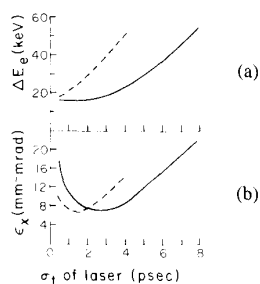
Fig. 6. (a) The beam energy spread ΔE_e and (b) the transverse emittance ϵ_x at the exit of the gun as a function of the laser pulse length. The solid (dashed) curves are for a peak RF field at a cathode of 100 (200) MV/m.
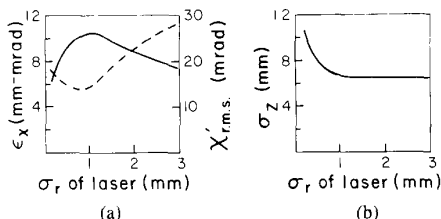

Fig. 7. (a) The transverse emittance ϵ_x (solid curve), and the rms beam divergence (dashed curve) as a function of the radius of the laser spot size on the cathode. (b) The rms bunch length at the exit of the gun as a function of laser spot size. Other parameters are as in Table I.
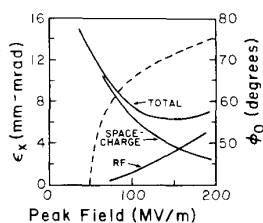

Fig. 8. The transverse emittance (solid curves) as a function of the peak RF field on the cathode, and the optimum phase (dashed curve) for the laser pulse to strike the cathode. Other parameters are as in Table I.
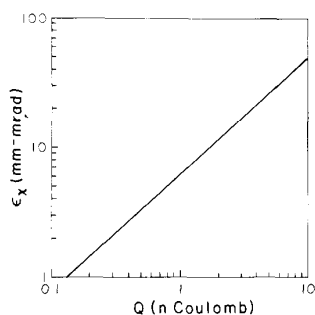

Fig. 9. The transverse emittance ϵ_x as a function of the charge of the electron bunch, with other parameters as in Table I.

walls. The π-mode and the 0-mode are found to be 2 MHz apart when the gun has no external coupling, as was also calculated by SUPERFISH.

The field profile along the z-axis has been measured by observing the frequency perturbations caused by a $\frac{7}{16}$-in teflon sphere. The results shown in Fig. 10 agree well (after tuning of the two cells) with the SUPERFISH cal-
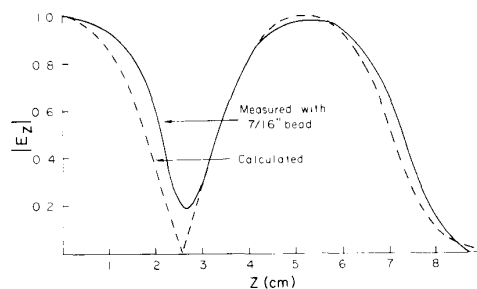

Fig. 10. $|E_z|$ as a function of position z along the axis of the RF gun. The solid curve was measured and the dashed curve was calculated.

culation. The bead size did not permit a clear demonstration of the zero-field point at the iris between the two cells.

An RF gun based on the present design is presently under construction.

APPENDIX A
FOURIER ANALYSIS OF THE RF FIELDS

We consider here a general form for standing-wave fields in a cavity (or extended structure) with cylindrical symmetry. From this form we can anticipate that a series of cavities operated in π-mode will impart the least apparent growth to the transverse emittance of the beam.

The unit cell to be analyzed (see Fig. 11) extends over $-d \leq z \leq d$. We suppose that $z = 0$ is a symmetry plane, and hence an appropriate expansion for E_z that also satisfies the wave equation is

$$E_z(r, z, t) = \sum_{n=1}^{\infty} a_n I_0(k_n r)$$
$$\cos\left(2n - n_0\right)\frac{\pi z}{2d} \sin\left(\omega t + \phi_0\right)$$

with

$$k_n^2 = \left(\left(2n - n_0\right)\frac{\pi}{2d}\right)^2 - \left(\frac{\omega}{c}\right)^2$$

The case $n_0 = 1$ corresponds to the condition that $E_z(r, d, t) = 0$, while $n_0 = 2$ corresponds to $\partial E_z(r, d, t)/\partial z = 0$, as shown in Fig. 11.

The radial electric field and azimuthal magnetic field then have the expansions

$$E_r(r, z, t) = \frac{\pi r}{4d} \sum_{n=1}^{\infty} \left(2n - n_0\right)a_n \tilde{I}_1(k_n r)$$
$$\sin\left(2n - n_0\right)\frac{\pi z}{2d} \sin\left(\omega t + \phi_0\right)$$

and

$$B_\theta(r, z, t) = \frac{\pi r}{\lambda} \sum_{n=1}^{\infty} a_n \tilde{I}_1(k_n r)$$
$$\cos\left(2n - n_0\right)\frac{\pi z}{2d} \cos\left(\omega t + \phi_0\right)$$
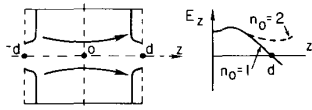
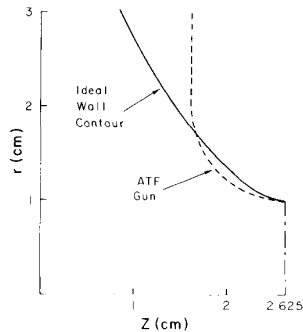Fig. 11. Geometry of the RF structure considered in the Fourier analysis.

Fig. 12. Section through a half-cell of an ideal RF cavity (solid curve) and of the ATF cavity (dashed curve).

where

$$\tilde{I}_1(z) \equiv \frac{2I_1(z)}{z} = 1 + \frac{(z/2)^2}{1!2!} + \frac{(z/2)^4}{2!3!} + \cdots .$$

If E_r and B_θ are nonlinear in r, then the RF fields will cause a distortion of the phase space that cannot be corrected later with linear optics. From our expansion for E_r we see that linear behavior can only be obtained when $k_n = 0$. The most relevant possibility is for $n = 1$ and also $n_0 = 1$, which leads to the requirement $d = \lambda/4$. The RF fields are then

$$E_z = E_0 \cos \frac{\pi z}{2d} \sin (\omega t + \phi_0)$$

$$E_r = \frac{\pi r}{4d} E_0 \sin \frac{\pi z}{2d} \sin (\omega t + \phi_0)$$

$$B_\theta = \frac{\pi r}{4d} E_0 \cos \frac{\pi z}{2d} \cos (\omega t + \phi_0).$$

The conditions that the full cell length be $\lambda/2$ and that E_z vanish at the cell boundaries are exactly those of the operation of a π-mode structure. Note that the shaping of E_z to $\cos \pi z/2d$ near the z axis actually requires an aperture (beam port) in the cell wall.

Surfaces perpendicular to the electric field lines have the form

$$r^2 = a^2 - \left(\frac{4d}{\pi}\right)^2 \log \left(\sin \frac{\pi z}{2d}\right)$$

where a is the radius of the aperture at $z = d$. Near $z = d$ the curve is a hyperbola. As $z \to 0$, $r \to \infty$, so no finite cavity can support these fields. Fig. 12 shows such a curve for the case $d = 2.625$ cm and $a = 1.0$ cm. The electrode shape for the ATF gun is also shown for comparison. For the ATF gun the Fourier coefficients of all higher harmonics are less than 15 percent of the fundamental.

APPENDIX B
THE POINT-BY-POINT SPACE-CHARGE CALCULATION

A point-by-point space-charge calculation was written to replace the usual approximation found in program PARMELA.

In the new calculation the forces due to the electromagnetic fields at each simulated particle are evaluated based on the present positions and velocities of all other simulated particles. Options are available to calculate fields due to images in the cathode, and/or in a beam pipe. For n simulated particles, n^2 fields must be evaluated at each step in the beam transport, so the space-charge calculation is somewhat time consuming.

The use of only the present positions and velocities in the calculation is not strictly correct, but a convenient approximation. Here we estimate the error due to this procedure.

We evaluate the fields due to another charge using

$$E = \frac{Qr}{\gamma^2 s^3}$$

and

$$B = \beta \times E$$

where

$$s = r(1 - \beta^2 \sin^2 \theta)^{1/2}$$

r is the vector from the present position of charge Q to the observer, $\beta = v/c$ is the present velocity of the charge, and θ is the angle between r and β. This expression would be exact if the charge had a uniform velocity.

In case the charge is accelerating the electric field at the observer may be written

$$E = \frac{Qr_{\mathrm{eff}}}{\gamma_{\mathrm{ret}}^2 s_{\mathrm{eff}}^3} + \frac{Qr_{\mathrm{ret}} \times (r_{\mathrm{eff}} \times \dot{\beta}_{\mathrm{ret}})}{cs_{\mathrm{eff}}^3}$$

where the subscript ret means the quantity should be evaluated at the retarded coordinates of the charge, and the subscript eff means the quantity should be evaluated by extrapolating from the retarded time to the present assuming the retarded velocity remains constant (see, for example, [10]).

On comparing the exact and approximate expressions for E we see that the relative error in the approximation is

$$\frac{\delta E}{E} \approx \frac{\gamma^2 \dot{\beta} r}{c}.$$

Now the acceleration $\dot{\beta}$ is largely due to the applied RF field E_0, so we have

$$\frac{d\gamma\beta}{dt} = \gamma^3 \dot{\beta} = \frac{eE_0}{mc} = \frac{2\pi\eta c}{\lambda}$$

where $\eta = eE_0/m\omega c \sim 1$ for our RF fields, λ is the RF wavelength, and we suppose β is parallel to E_0. Then

$$\frac{\delta E}{E} \approx \frac{2\pi\eta}{\gamma} \frac{r}{\lambda}.$$

Thus, our use of the present parameters of the charge is in significant error only when the distance to the charge is of the order of an RF wavelength. But then the force due to the charge is so small as to be irrelevant.

At a frequency of 2856 MHz, the wavelength λ is 10.5 cm, and then for $E_0 = 100$ MV/m we have $\eta \sim 3$. In a bunch of 5 ps full width, a typical value of r is 1 mm. Hence, we may expect our use of the present positions and velocities to yield an accuracy of 20 percent in the space-charge calculation.

The charge Q on each simulated particle is taken as the electron charge e multiplied by the ratio of the number of electrons in the bunch to the number of particles used in the simulation. As the number of simulated particles is typically less than 1000, the value of Q is quite large. Fluctuations in the simulation may then lead to overestimation of the space-charge force between nearby charges. We introduce a screening radius R of 1.75 times the average distance to the nearest charge, and scale the simulated charge by Qr/R for pairs with separation $r < R$. This prescription proved stable against variation of the number of simulated particles between 100 and 5000.

The present space-charge calculation has been compared with a result obtained with the program MASK [11], which uses a Green's function technique to evaluate the fields from the electron bunch. Both programs calculated the same gun geometry, and both assumed a hard-edge cylinder of charge rather than a Gaussian ellipsoid. MASK gave a result for the space-charge emittance growth only one half that of PARMELA. While the reasons for the discrepancy remain unclear, the comparison is consistent with the general lore that space-charge calculations are reliable only to a factor of two.

ACKNOWLEDGMENT

REFERENCES

[1] R. B. Palmer, "A laser-driven grating linac," *Part. Accel.*, vol. 11, pp. 81–90, 1980.
[2] E. Courant *et al.*, "Proposal for the design and construction of an IFEL accelerator demonstration stage," Brookhaven Nat. Lab., 1987.
[3] R. C. Fernow *et al.*, "Proposal for an experimental study of nonlinear Thomson scattering," Princeton Univ. preprint DOE/ER/3072-39, 1986.
[4] J. S. Fraser *et al.*, "Photocathodes in accelerator applications," in *Proc. IEEE Particle Accelerator Conf.*, (Washington, DC, Mar. 16–19, 1987), pp. 1705–1709.
[5] M. E. Jones and W. K. Peter, "Particle-in-cell simulations of the lasertron," *IEEE Trans. Nucl. Sci.*, vol. NS-32, no. 5, pp. 1794–1796, 1985.
[6] M. T. Menzel and H. K. Stokes, "User's guide for the POISSON/SUPERFISH group of codes," Los Alamos Nat. Lab. Rep. LA-UR-87-115, Jan. 1987.
[7] J. Fischer and T. Rao, "UV photoemission studies from metal photocathodes for particle accelerators," in *Proc. Workshop Pulsed Power Tech. for Future Accelerators* (Erice, Italy, Mar. 1988), to be published.
[8] K. Batchelor *et al.*, "Development of a high brightness electron gun for the Accelerator Test Facility at Brookhaven National Laboratory," in *Proc. 1st European Particle Accelerator Conf.* (Rome, Italy, June 1988), to be published.
[9] H. G. Kirk, private communication.
[10] W. K. Panofsky and M. Phillips, *Classical Electricity and Magnetism*, 2nd ed. Reading, MA: Addison-Wesley, 1962, pp. 356–357.
[11] R. Koul, "Some recent studies of a π-mode RF gun," Brookhaven Nat. Lab. preprint, Sept. 1988.

*

Kirk T. McDonald received the Ph.D. degree in physics from the California Institute of Technology in 1972.

After postdoctoral research at CERN, Switzerland, and the University of Chicago, he is now a Professor of Physics at Princeton University. He has primarily worked in the field of experimental high-energy physics and has performed experiments at the Caltech electron synchrotron, the LBL 184" cyclotron, the CERN Intersecting Storage Rings, at Fermilab, and at the Brookhaven Alternating Gradient Synchrotron. The general theme of these studies has been the quark structure of matter. Recently, he has become involved in studies of nonlinear QED effects of electrons in intense laser fields. The design of the high-brightness electron gun is part of the effort to build a facility to investigate various novels aspects of electron–photon interactions.